An improved single crystal adsorption calorimeter for determining gas adsorption and reaction energies on complex model catalysts

Jan-Henrik Fischer-Wolfarth,[1] Jens Hartmann,[1] Jason A. Farmer,[2] J. Manuel Flores-Camacho,[1] Charles T. Campbell,[2] Swetlana Schauermann,[1,a)] and Hans-Joachim Freund[1]

[1]*Fritz-Haber-Institut der Max-Planck-Gesellschaft, Faradayweg 4-6, 14195 Berlin, Germany*
[2]*Department of Chemistry, University of Washington, Box 351700, Seattle, Washington 98195-1700, USA*

(Received 3 September 2010; accepted 29 December 2010; published online 17 February 2011)

A new ultrahigh vacuum microcalorimeter for measuring heats of adsorption and adsorption-induced surface reactions on complex single crystal-based model surfaces is described. It has been specifically designed to study the interaction of gaseous molecules with well-defined model catalysts consisting of metal nanoparticles supported on single crystal surfaces or epitaxial thin oxide films grown on single crystals. The detection principle is based on the previously described measurement of the temperature rise upon adsorption of gaseous molecules by use of a pyroelectric polymer ribbon, which is brought into mechanical/thermal contact with the back side of the thin single crystal. The instrument includes (i) a preparation chamber providing the required equipment to prepare supported model catalysts involving well-defined nanoparticles on clean single crystal surfaces and to characterize them using surface analysis techniques and *in situ* reflectivity measurements and (ii) the adsorption/reaction chamber containing a molecular beam, a pyroelectric heat detector, and calibration tools for determining the absolute reactant fluxes and adsorption heats. The molecular beam is produced by a differentially pumped source based on a multichannel array capable of providing variable fluxes of both high and low vapor pressure gaseous molecules in the range of 0.005–1.5 $\times$ 10^{15} molecules cm^{-2} s^{-1} and is modulated by means of the computer-controlled chopper with the shortest pulse length of 150 ms. The calorimetric measurements of adsorption and reaction heats can be performed in a broad temperature range from 100 to 300 K. A novel vibrational isolation method for the pyroelectric detector is introduced for the reduction of acoustic noise. The detector shows a pulse-to-pulse standard deviation $\leq$15 nJ when heat pulses in the range of 190–3600 nJ are applied to the sample surface with a chopped laser. Particularly for CO adsorption on Pt(111), the energy input of 15 nJ (or 120 nJ cm^{-2}) corresponds to the detection limit for adsorption of less than 1.5 $\times$ 10^{12} CO molecules cm^{-2} or less than 0.1% of the monolayer coverage (with respect to the 1.5 $\times$ 10^{15} surface Pt atoms cm^{-2}). The absolute accuracy in energy is within $\sim$7%–9%. As a test of the new calorimeter, the adsorption heats of CO on Pt(111) at different temperatures were measured and compared to previously obtained calorimetric data at 300 K. © *2011 American Institute of Physics*. [doi:10.1063/1.3544020]

I. INTRODUCTION

Determination of the strength of adsorbate–surface and lateral adsorbate–adsorbate interactions is an important fundamental issue in surface science research and an essential prerequisite for understanding real catalytic processes. The energetics of such interactions can be quantified by measuring the amount of heat released upon adsorption and/or reaction of the gas phase molecules on the clean and adsorbate-precovered surfaces. The traditionally used experimental techniques for probing the energetics of adsorption—temperature-programmed desorption (TPD) and equilibrium adsorption isotherm measurements—provide reliable results only for systems with fully reversible adsorption, i.e., most of the catalytically relevant processes, involving dissociation, reaction with coadsorbates, clustering or diffusion into bulk, cannot be probed by these methods correctly.

These restrictions can be overcome by using a novel method of single crystal adsorption calorimetry (SCAC), which was invented a decade ago by Borroni-Bird and King[1] and further developed by Campbell *et al.*[2–5] This method allows us to directly measure heats of adsorption and reaction of gaseous molecules interacting with well-defined surfaces and can be applied not only under the adsorption–desorption equilibrium conditions but also in situations where it is impossible to establish adsorption–desorption equilibrium, e.g., when the adsorbed molecule of interest would dissociate on the surface before reaching a temperature high enough for desorption. Such data provide highly important benchmarks for theoretical calculations and are generally not available at the moment. SCAC was successfully applied on metal single crystals to study the energetics of gas–surface interactions for different molecular adsorbates.[3,5,6] Also the interaction strength of metals with metal single crystals and oxide surfaces was addressed.[2,3]

Despite the considerable advances in understanding gas–surface interactions relevant to catalysis that have been

a)Author to whom correspondence should be addressed. Electronic mail: schauermann@fhi-berlin.mpg.de. Tel.: +4930-8413 4142.

 © 2011 American Institute of Physics

Downloaded 25 May 2011 to 141.14.132.216. Redistribution subject to AIP license or copyright; see http://rsi.aip.org/about/rights_and_permissions

achieved studying single crystal metal surfaces, many phenomena inherent to realistic supported catalysts (e.g., metal nanoparticles dispersed across an oxide support) cannot be addressed on such simplified model systems, since they do not reproduce some important structural properties that can affect catalytic activity, such as different particle sizes, presence of a support, and sites at the metal-support boundary. Particularly for the catalytic applications, knowledge on the correlation between the strength of the adsorbate–catalyst interaction and the detailed structure of the catalytically active surface is an essential prerequisite for unraveling the factors governing the activity and the selectivity of the catalyst. At the present time, this fundamental information is not available. The vast complexity of industrial catalysts is the primary impediment to the acquisition of this information, which precludes detailed structural studies by standard surface science techniques.[7] Recently, a variety of well-defined model systems have been developed, consisting of metal nanoparticles supported on a well-ordered oxide film grown on metal single crystal.[8–10] This approach allows one to controllably vary the degree of complexity of supported catalysts and enables a detailed characterization of their surface structure without loosing the catalytically important structural properties of the realistic supported systems, such as industrial catalysts. Several examples of model catalysts have been characterized in our group with respect to their geometric and electronic structures as well as their reactivity behavior.[11–14]

In order to link detailed knowledge on the structural properties of the catalyst to the energetics of the gas–surface interaction, we have built a new microcalorimetric experiment based on the pyroelectric heat detection technique of Campbell *et al.*[2] and combined it with facilities for the preparation of well-defined supported model catalysts. Additionally, instrumentation for TPD spectroscopy was added to compare SCAC measured adsorption enthalpies with the energetics of the reverse desorption processes. The specific capabilities required for such measurements are the following.

(1) Sample preparation and characterization. The tools for preparation and characterization of a variety of model supported catalysts have to be integrated. Particularly, the ability to deposit several metals to prepare different metal oxides and/or metal nanoparticles is required. A sample transfer from the preparation chamber into the microcalorimetry detector under ultrahigh vacuum (UHV) is essential.
(2) *In situ* reflectivity measurement. The reflectivity of the sample is a crucial parameter for the calibration of the absolute value of deposited energy, and it changes when changing the structural properties of the model catalyst. Thus, a method for measuring the reflectivity of the model supported catalysts prepared under UHV conditions *in situ* has to be integrated.
(3) Molecular beam source. The molecular beam source should allow the molecular flux to be varied over the largest possible range. The molecular beam must be well-collimated and pulsed with a variable modulation frequency with pulse length in the order of 0.1 s. The pulsed molecular beam must be produced in a way that generates only low intensity vibrations in the UHV chamber since the pyroelectric heat detector inherently possesses a high piezoelectric coefficient and hence is very sensitive to mechanical vibrations. The beam must be suitable for using a large variety of gases: both "light" gases with high vapor pressure, such as CO and ethylene, used in the studies of King *et al.*[6] as well as large molecules with low vapor pressure ($>10^{-2}$ mbar) such as benzene applied in the experimental setup of Campbell *et al.*[15] For more complex experiments requiring exposure to several reactants, it is necessary to provide the ability to dose more than one reactant via the molecular beam.
(4) Microcalorimetric detection of adsorption heats has to be realized in a broad temperature range from 100 to 300 K, which requires high thermal stability (on the order of mK) on the time scale of tens of minutes. High sensitivity of the pyroelectric detector to the mechanical vibrations requires the best possible vibrational isolation of the microcalorimeter from the UHV chamber.
(5) *In situ* calibration techniques for determining the absolute values of beam fluxes and absolute adsorption/reaction enthalpies must include (i) a beam monitor for measuring the absolute reactant flux and (ii) a UHV-integrated photodiode for *in situ* measuring the laser power for the absolute energy calibration. It should be possible to place all tools at the very same position with respect to the molecular beam to reduce systematic errors.
(6) Combination of direct energy measurement by microcalorimetry with TPD requires integration of two different sample types. Single crystals of 1 μm thickness are used for microcalorimetric measurements, but their highly nonuniform temperature profile and restrictions with respect to accurate temperature measurements during rapid heating makes TPD difficult. For this purpose, a second sample of about 1 mm thickness needs to be integrated.

We describe here a relatively compact apparatus that meets these requirements.

There are two general types of detection methods applied in SCAC instruments that have been described in the literature for the direct measurement of adsorption enthalpies of molecular species on single crystal surfaces.[1,5,16] The SCAC setup originally developed by Borroni-Bird and King[1] consists of a pulsed supersonic molecular beam, an ~200 nm thick single crystal sample, and a detector based on infrared optical pyrometry. Figure 1 shows a scheme of this method: in a microcalorimetric experiment a pulse of gas from a chopped molecular beam impinges on an ultrathin single crystal surface. A fraction of the molecules striking the surface adsorbs, causing a transient heat input and a transient temperature rise. The blackbody radiation from the back of the single crystal that is associated with this transient temperature rise can be quantified by using a sensitive infrared detector. The calibration of the absolute value of adsorbed heat is realized by measuring the heat signal from a diffuse He–Ne laser at 633 nm of known power, which is chopped and collimated in an

Downloaded 25 May 2011 to 141.14.132.216. Redistribution subject to AIP license or copyright; see http://rsi.aip.org/about/rights_and_permissions

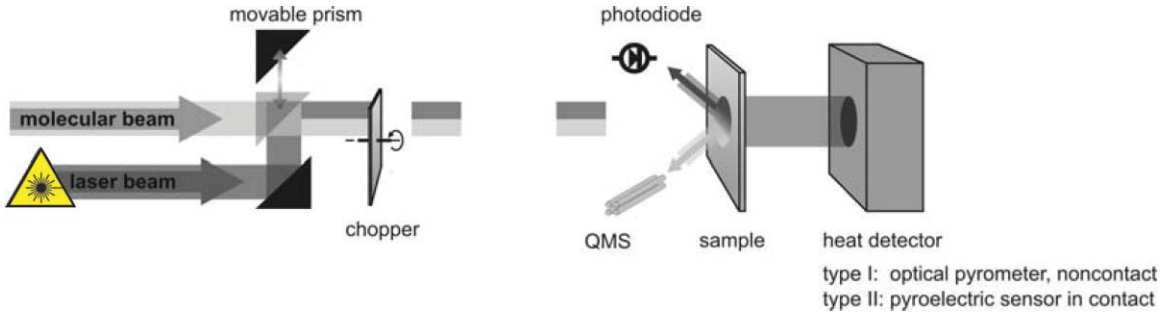

FIG. 1. (Color online) Schematic diagram showing the working principle of a single crystal adsorption calorimeter.

identical way as the gas beam before impinging on the sample surface. Additionally, a sticking coefficient measurement is performed by King–Wells method[17] to determine what fraction of molecules in each pulse sticks to the surface and contributes to the observed heat. Therefore, the adsorption heats can be expressed as per mole of gas adsorbed and the absolute surface coverage can be calculated. This experimental setup based on optical pyrometry has a number of disadvantages. The sensitivity of the infrared detection method decreases substantially at temperatures less than 300 K, making low-temperature studies impossible. Additionally, the very thin samples of ~200 nm are difficult to handle and not all materials are mechanically stable as free standing crystals at such thicknesses, which restricts the range of the materials suitable for investigation.

These restrictions were overcome in the latter modification of SCAC based on a new heat detector developed by Campbell *et al.*[2] In this detection method the transient temperature rise is measured by an ~9 μm thick β-polyvinylidene fluoride (PVDF) pyroelectric ribbon coated on the both sides with a metal, providing electric contacts. The pyroelectric ribbon produces a face-to-face voltage signal across the ribbon in response to a heat input. The generated voltage is measured by a high impedance amplifier circuit.[2,18] The higher sensitivity of the pyroelectric detection method allowed for the use of thicker single crystals of 1 to ~125 μm.[4] The detection method also provides high sensitivity at low temperatures, making it possible to considerably extend the range of adsorbates and reaction intermediates that can be investigated. For example, the details of adsorption and stepwise decomposition of large organic molecules have recently been revealed on a Pt(111) single crystal at temperatures close to 100 K.[3,19] This type of calorimeter was also successfully applied for studying adsorption of metal atoms on the different kinds of substrates, including oxide films grown on single crystal surfaces.[3] For this type of measurements a special atomic beam was implemented, which allows controlled deposition of metal atoms from the heated metal source.

Two parameters critically influence the calibration procedure: the absolute intensity of the laser light and the reflectivity of the sample. To obtain an accurate value of the energy deposited with a laser pulse, it is necessary to precisely measure these parameters *in situ*.

In this paper, we describe a new single crystal adsorption calorimetry apparatus, which was designed for a direct measurement of gas-phase adsorption and reaction enthalpies on well-defined supported model catalysts. Based on the previously developed highly sensitive pyroelectric detector, the heat input to the sample due to adsorption is detected by using a pyroelectric polymeric PVDF-ribbon pressed against the back of the ultrathin single crystal. The UHV system is divided into two separate chambers.

(1) The preparation and characterization chamber contains all necessary tools for preparation of various types of oxide films, which are grown on single crystal surfaces, as well as for deposition of desirable metal to form supported nanoparticles. The preparation can be carried out on both ultrathin single crystals (~1 μm) for the microcalorimetric measurements and on the thicker (~1 mm) single crystals for the TPD experiments. The ability to carry out desorption studies on the identically prepared surfaces allows for a direct comparison of adsorption energies obtained by both methods. For precise *in situ* measurement of optical reflectivity of the model surfaces, a new reflectivity setup was implemented in the preparation chamber, which contains five absolute standards for calibration purposes.

(2) The main chamber contains a differentially pumped effusive molecular beam source, which can be chopped with variable frequency and provides flexible modulation of the flux intensities by varying the expansion conditions. This is a more versatile molecular beam than the ones applied in the other calorimetric setups,[1,5] which allows the use of both high and low vapor pressure gases. The heat detector together with the sample can be cooled down by liquid nitrogen or precooled Ar, enabling flexible temperature variation between 100 and 300 K. Long-term temperature stability is reached on a time scale of several hours. A new mechanism for driving the heat detector into contact to the single crystal sample was developed, which allows reduction of the mechanical and thermal contacts of the calorimeter to the vacuum chamber. This mechanism provides potential advantages over previous designs including possibility for improved vibrational isolation, better thermal stability, and faster thermal equilibration of the sample with the detector. Additional vibrational isolation of the entire calorimeter was implemented to reduce piezoelectric noise, which is inherent to any pyroelectric material. *In situ* calibration tools—

Downloaded 25 May 2011 to 141.14.132.216. Redistribution subject to AIP license or copyright; see http://rsi.aip.org/about/rights_and_permissions

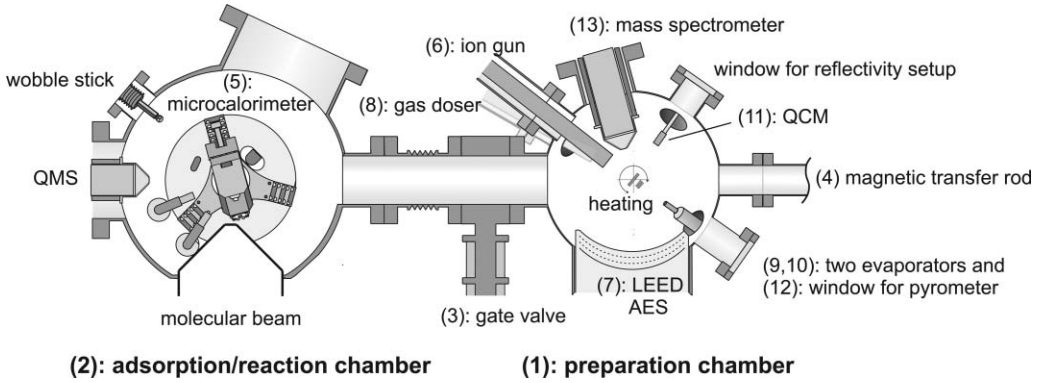

FIG. 2. Schematic overview of the experimental setup. The labeled components are (1) preparation chamber, (2) adsorption/reaction chamber, (3) gate valve, (4) magnetic transfer rod, (5) microcalorimeter, (6) ion gun, (7) optics for LEED and AES, (8) gas doser, (9) and (10) two metal evaporators, (11) QCM, (12) port for pyrometer, and (13) mass spectrometer.

a beam monitor for determining the absolute fluxes of the gas-phase molecules and a photodiode for measuring the laser light intensity—are additionally integrated into the chamber. All three types of detectors—the heat detector, the beam monitor, and the photodiode—are mounted on a rotatable differentially pumped platform, which enables their precise positioning in front of the molecular beam and thus reduces the systematic errors. The residual gases and sticking probabilities are measured using a nondifferentially pumped quadrupole mass spectrometer (QMS).

In Sec. II we will first provide a general overview over the apparatus and a more detailed description of the newly developed components and technical details. In Sec. III the first experimental test data will be presented, which compare the adsorption energy values measured in this apparatus with previously published data.

II. SYSTEM DESIGN

A general overview of the experimental apparatus is shown in Fig. 2. The preparation of complex model catalysts requires several preparation methods. Because of spatial limitations of the UHV chamber containing a microcalorimetric detector, we have separated the system into a preparation chamber (1) and an adsorption/reaction (2) chamber. Both chambers are independent UHV systems separated by a gate valve (3). Two manipulators (placed in the center of each chamber, not shown) and a translational rod (4) are used for sample manipulation and transfer between the chambers and the microcalorimeter (5).

The thin ($\sim$1 μm) and thick ($\sim$1 mm) single crystal samples are mounted on Mo sample holders, which can be fixed on both manipulators in the preparation and adsorption/reaction chamber. The thin single crystal sample is employed in microcalorimetric measurements, whereas the thick sample is used for *in situ* reflectivity (see Sec. II C) and TPD measurements.

A. Sample preparation chamber

The preparation chamber is pumped by a 500 l/s turbo molecular pump (TMP) (Pfeiffer, TMU 521 P), which is capable of reaching and maintaining a base pressure of 1×10^{-10} mbar. A differentially pumped ion gun (Omicron, ISE 10) (6) and a low energy electron diffraction (LEED)/Auger electron spectroscopy (AES) system (SPECS, ErLEED) (7) are used for sample cleaning and characterization of the single crystal and model supported catalysts. In order to reduce the background pressure rise during preparation, a gas dosing system (8) was implemented. Preparation of complex model catalysts under UHV conditions can be accomplished using physical vapor deposition of different metal components, which is realized by two electron beam evaporators (Omicron, EFM 3) (9,10). In order to avoid undesirable damage of the samples by ions produced in the electron beam evaporator source, a retarding voltage equal to the acceleration potential of the evaporator is applied to the sample during preparation to decelerate those ions. The evaporator fluxes are calibrated using a quartz crystal microbalance (QCM) (Sigma Instruments) (11).

A sample manipulator with one rotational and three translational degrees of freedom is mounted in the center of the preparation chamber and can carry two samples. A thin ($\sim$1 μm, 12 $\times$ 16.5 mm) single crystal sample[19] is mounted onto a transferable Mo sample holder by a Ta sheet with a round hole (diameter 8 mm) in the center. The sample is sandwiched between the Ta sheet and the Mo sample holder, and this assembly is then spot-welded together. Two springs, placed on both sides of the transferable sample holder, hold the sample firmly in place but allow for removing the sample holder from the manipulator using a wobble stick. A translational rod (4), equipped with three units for holding samples, can be used to receive the sample holder from the wobble stick (not shown) and to transfer it into the adsorption/reaction chamber (2), where another wobble stick (not shown) is placed for sample handling. The sample can be cooled to 90 K using liquid nitrogen and heated up to $\sim$1300 K. Heating of the sample is realized by electron bombardment from a flat filament of a commercial halogen bulb, which is situated approximately 10 mm behind the sample holder and is aligned parallel to the sample to ensure homogeneous heating. A thermocouple cannot be mounted to such a thin single crystal as used here; therefore, a pyrometer (Sensortherm MP

Downloaded 25 May 2011 to 141.14.132.216. Redistribution subject to AIP license or copyright; see http://rsi.aip.org/about/rights_and_permissions

25) (12) is used for temperature measurement during preparation in the range between 450 and 1300 K. For the thick (1 mm) single crystal sample, the temperature is measured using a type-K thermocouple, which is spot-welded to the crystal edge. The thermocouple wires are electrically connected to the manipulator by sliding contacts.

Temperature-programmed desorption can be performed in the preparation chamber by means of a QMS (Hiden, Halo 201) (13) equipped with a gold plated aperture. A LABVIEW-based temperature ramp generator allows heating rates of up to 10 K/s.

B. Setup for reflectivity measurement in sample preparation chamber

The absolute energy calibration relies on accurate knowledge of the energy input deposited into the sample by a laser pulse during the calibration procedure. Since only a part of the incoming laser light is absorbed by the sample, the energy input can be calculated only if the total reflectivity of the sample is known. For the *in situ* prepared model supported catalysts, there are no reliable literature data on their reflectivity. For this reason, it is necessary to precisely determine the reflectivity of the investigated samples *in situ* under UHV conditions for each preparation.

To obtain accurate values of the reflectivity of the model supported catalysts, we implemented a special setup that allows for *in situ* measurements immediately after preparation. Figure 3 shows a schematic representation of the arrangement for the reflectivity measurement in the preparation chamber. A He–Ne laser (Lasos, 632.8 nm, 2 mW, continuous wave) (1) is mounted in front of a 70 mm conflate window (2) pointing toward the center of the chamber. The sample or the references can be placed at this position for reflectivity measurements and calibration, respectively. After passing through the borosilicate window (2), the laser light impinges on the sample surface (3) at an angle of about ~5° relative to the surface normal. The reflected intensity is measured by the main photodiode (Silicon Sensor, PS100-2) (4) placed next to the laser. The laser power fluctuations are simultaneously monitored via splitting the laser beam by a beam splitter (5) and detecting the reflected component by a separate photodiode (Silicon Sensor, PS95-4) (6). The use of a polarization dependent beam splitter requires an additional linear polarizer (7),

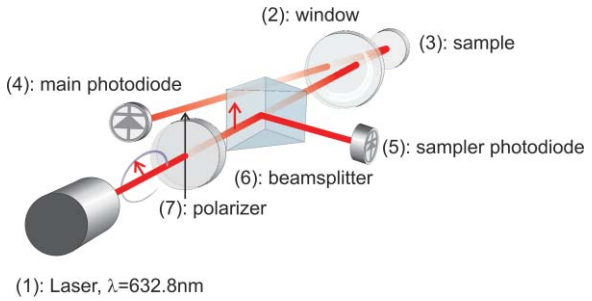

FIG. 3. (Color online) Schematic overview over the setup for reflectivity measurements. The labeled components are (1) He–Ne laser, (2) chamber window, (3) sample, (4) main photodiode, (5) sampler photodiode, (6) beamsplitter, and (7) polarizer.

since the polarization of the initial laser beam changes due to, e.g., mode sweeping, mode competition, alignment changes, etc. Inside the preparation chamber five dielectric mirrors (LayerTec) of known reflectance are installed on the manipulator, which are used as calibration references.

C. Adsorption/reaction chamber

The adsorption/reaction chamber is designed for simultaneous microcalorimetry and sticking probability measurements. Figure 4 shows an overview of the experimental arrangement of the adsorption/reaction chamber. After the preparation the sample is transferred into the adsorption/reaction chamber by the translational rod. The sample can reside either in the microcalorimeter or on the manipulator placed in the center of the adsorption/reaction chamber, which possesses one rotational and three translational degrees of freedom (the manipulator is not shown). The chamber (Tectra) is pumped by a 500 l/s TMP (Pfeiffer, TMU 521 P), resulting in a base pressure of 2×10^{-10} mbar.

This chamber includes a high-flux effusive molecular beam (1) with an integrated chopper and the tools for calibration purposes (for details see Sec. II E). A differentially pumped rotatable platform (2) mounted in the center of the adsorption/reaction chamber carries three types of detectors: the microcalorimeter (3) for the measurement of adsorption/reaction heats, a UHV-compatible photodiode (4) for *in situ* measurements of the absolute laser intensity, and a beam monitor (5) for the measurement of the absolute molecular beam fluxes.

The microcalorimeter consists of two main parts—an electrically isolated Mo sample holder mounting (6) and a detector head (7), both mounted on a Cu platform (8) (for

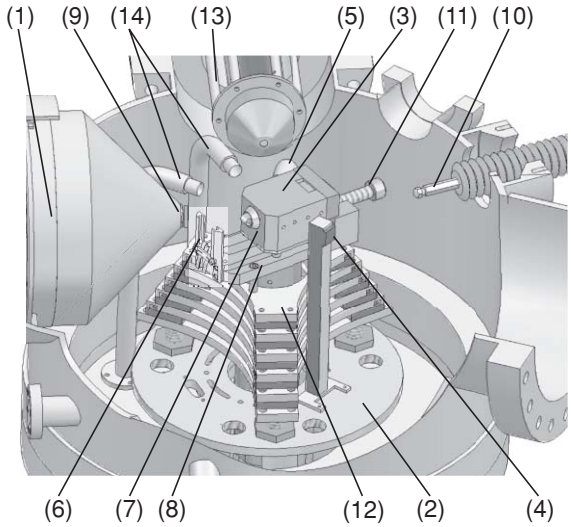

FIG. 4. Overview of the main components in the adsorption/reaction chamber. The labeled components are (1) molecular beam source, (2) rotatable platform, (3) microcalorimeter, (4) *in situ* photodiode, (5) beam monitor, (6) sample holder mounting, (7) detector head of the microcalorimeter, (8) Cu platform carrying the sample holder mounting and the detector, (9) outer molecular beam aperture, (10) Allen wrench mounted on wobble stick, (11) translation screw, (12) vibration damping stack, (13) QMS, and (14) two gas dosers.

Downloaded 25 May 2011 to 141.14.132.216. Redistribution subject to AIP license or copyright; see http://rsi.aip.org/about/rights_and_permissions

further details on the microcalorimeter setup, see Sec. II D). The position of the Mo sample holder mounting (6) is fixed on the Cu platform; the movable detector head (7) can slide along in order to approach the sample positioned in the sample holder mounting (6) and establish a mechanical/thermal contact to the back of the thin single crystal. In the working position the sample holder mounting (6) with an inserted thin single crystal sample is placed in front of the outer molecular beam aperture (9) at a distance of 4 mm. The detector head (7) can be moved and pressed toward the sample by using an Allen wrench fixed on a rotatable wobble stick (10) and a translation screw (11) mounted into the detector on the back side. After the contact with the sample is established, the wobble stick (10) can be removed from the detector head, so that the entire calorimeter becomes mechanically decoupled from the outer chamber walls and remains connected only to the vibration damping stack (12) installed on the rotatable platform (2). The Cu platform and the entire microcalorimeter can be cooled down with liquid nitrogen or with a cooled gas to cryogenic temperatures. Prior to the beginning of the measurement, the sample has to be shielded from the molecular beam in order to obtain a reference signal for the sticking probability analysis by King–Wells method.[17] For this purpose, a gold flag (not shown) can be positioned between the sample and the outer molecular beam aperture (9). For the measurement of the molecular beam flux and the laser intensity calibration, the rotatable platform (2) can be rotated to bring the corresponding detectors—the beam monitor (5) and the photodiode (4)—in front of the molecular beam at a distance of 4 mm, which is precisely the same as the position of the one of the sample during the microcalorimetric measurement. Since only one coordinate—the rotation angle of the rotatable platform (2)—is varied to reach the working position, this procedure allows us to minimize the systematic errors due to misalignments of the different types of detectors.

For the sticking coefficient and reactivity measurements, the King and Wells method is used,[17] with a QMS (Hiden, HAL 301/3F PIC) (13) equipped with a gold plated aperture. For the reactivity measurements, two gas dosers (14) are available, allowing supply of two further reactants independently from the molecular beam source.

Sample heating in the adsorption/reaction chamber is realized by electron bombardment; additionally, the manipulator contains a separate filament which can be used for sample heating when it is positioned in the microcalorimeter.

D. Microcalorimeter and pyroelectric heat detection

Figure 5(a) shows a scheme of the microcalorimeter integrated into this apparatus. This instrument is an adaption of the microcalorimeter originally developed by Campbell *et al.*, described in detail elsewhere.[2] Here, we briefly describe the main components of the microcalorimeter and focus on the modifications of the previously developed calorimeter implemented in this apparatus. The sensitive element of the calorimeter is a pyroelectric β-PVDF ribbon (either an Al-coated 9 μm thick from Goodfellow or a Au/Cr-coated 6 μm thick from Piezotech) (1) polarized perpendicular to its faces and coated on both sides with metal for electrical contacts. The ribbon was cut into a 6.3 $\times$ 35 mm piece using ceramic scissors and etched according to the procedure described by Campbell *et al.*,[4] which reduces its capacitance (increasing the signal magnitude) and improves the signal-to-noise ratio. The ribbon is mounted into a detector housing (2), such that the ribbon forms a protruding 90° arch, and is electrically connected to an amplifier circuit. In the following, the assembly of the ribbon (1) and the detector housing (2) will be denoted as a detector head. Prior to the calorimetric measurement the detector head is mechanically driven along the Cu platform (3) using the translation screw (4) and the Allen wrench wobble stick [(10) in Fig. 4] toward the sample holder mounting (5) to make a gentle mechanical/thermal contact to the back side of the single crystal sample. When in contact with the sample holder, the highly flexible ribbon flattens, covering about 6 $\times$ 6 mm^2 of the

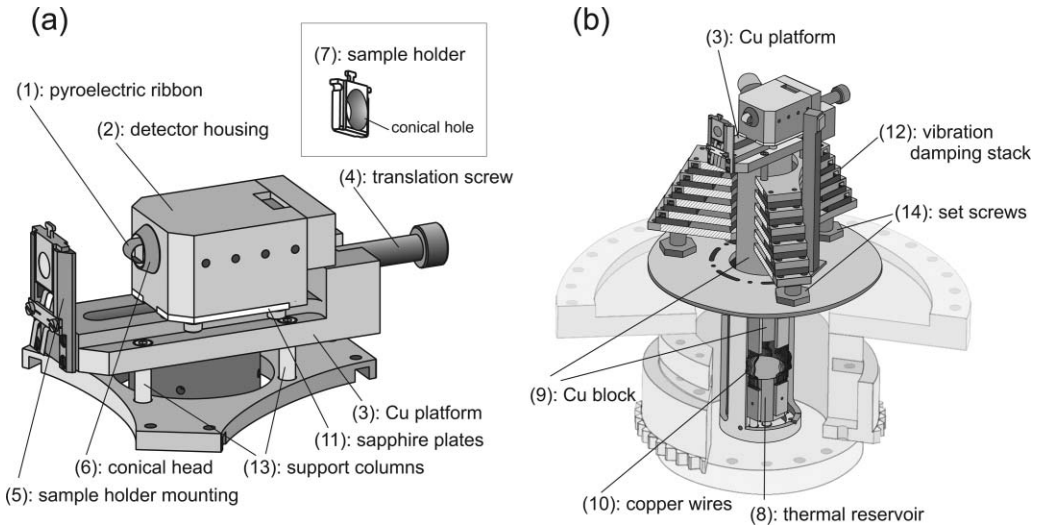

FIG. 5. Components of the microcalorimeter: (1) pyroelectric ribbon, (2) detector housing, (3) Cu platform carrying the detector housing and the sample holder mounting, (4) translation screw, (5) sample holder mounting, (6) conical head of the detector housing, (7) back view of the sample holder, (8) thermal reservoir, (9) Cu block, (10) copper wires, (11) sapphire plates, (12) vibration damping stack, (13) support columns, and (14) set screws.

Downloaded 25 May 2011 to 141.14.132.216. Redistribution subject to AIP license or copyright; see http://rsi.aip.org/about/rights_and_permissions

sample allowing for heat transfer from the sample to the ribbon. In order to ensure the reproducibility of the contact between the ribbon and the single crystal sample, the detector housing and the sample holder are designed in such a way that their contact is self-aligning and reproducible with respect to the location and extent of compression of the PVDF ribbon. This is achieved using a sample holder design similar to those used by Campbell *et al.*[4], consisting of a conical head (6) of the calorimetric detector and a corresponding negative form of the sample holder (7): the cone's outer diameter is designed to match exactly with a conical hole in the back of the sample holder [see inset in Fig. 5(a)]. While in contact with the sample, the ribbon is shielded from disturbing electromagnetic influences.

The temperature rise of the crystal, due to gas adsorption, induces a temperature change in the pyroelectric detector, causing it to develop a transient face-to-face voltage, which produces the measurable signal. The charge generated by a transient heat input is measured by a high impedance amplifier circuit, which has been described previously.[20] Reduction of electromagnetic noise in the chamber is achieved by the application of a guarding potential to the coaxial cables. A homemade differential preamplifier with a fixed amplification factor of 100 and a low-pass cut-off frequency of 10 kHz is directly connected to the chamber. A subsequent main amplifier incorporates an adjustable amplifier with a gain adjustable between 1 and 1000 and an adjustable band-pass filter with a fixed low-pass cut-off frequency of 10 Hz and a variable high-pass cut-off frequency of 0.2, 2, or 20 Hz. After the voltage is amplified it is recorded by a computer using a digital-to-analog convertor with a sampling frequency of 1 kHz.

The contact value, defined in terms of peak voltage rise per joule of absorbed heat (V/J), varies somewhat from contact-to-contact due to changes in the mechanical/thermal contact between the sample and the pyroelectric ribbon. Therefore, the detector voltage output must be calibrated for each contact directly after each heat measurement with pulses of He–Ne laser light at 632.8 nm of known intensity.

The microcalorimeter setup, including the detector head and the sample holder mounting, must be very thermally stable to enable the highest precision calorimetric measurements. Any drift in the temperature (voltage) during the calorimetric measurement will bias the peak-to-peak voltage measurement of the pyroelectric detector. An estimate of the required temperature stability, so as not to affect the measurement, can be calculated as follows: assuming a 1 μm thick Pt sample with the specific heat capacity of 2.86 J cm^{-3} K^{-1} (Ref. 21) and that the heated volume of the sample is localized in the area of the incident atomic beam, 0.125 cm^2, the temperature rise for a 0.02 monolayer (ML) CO pulse, corresponding to 3×10^{13} molecules cm^{-2}, with a heat of adsorption of 150 kJ mol^{-1} is $\sim$0.02 K. Given the pulse rise time of $\sim$0.2 s, the temperature stability is required to be below 0.002 K/s in order to not to contribute significantly to the measurement.

To achieve cryogenic temperatures and ensure the required temperature stability the Cu platform (3) carrying the detector head, the sample holder mounting and the sample holder are connected to a large (2 kg) Cu thermal reservoir (8) via a Cu block (9) and thin copper wires (10) [Fig. 5(b)]; this thermal reservoir provides sufficient temperature stability for hundreds of minutes. The thermal reservoir is a Cu vessel, which can be cooled by flowing liquid nitrogen or precooled gases through it via liquid-tight feedthroughs. The detector head is thermally connected to the Cu platform via sapphire plates (11) that serve as a slide bearing and the translation screw (4) made of Ag-based alloy. The good thermal contact between the sample holder and the detector head allows the sample to come quickly into thermal equilibrium with the whole calorimeter assembly. Particularly, the high thermal conductivity of the Ag translation screw was found to result in a fast temperature equilibration between the freshly cleaned sample (above 500 K) and the precooled detector head (typically 120–130 K) on a time scale of minutes. This fast thermal equilibration reduces waiting time and the associated surface contamination due to residual gas adsorption and is crucial for the overall accuracy of the calorimetric measurement.

In order to attenuate the vibration noise in the detector's signal, the Cu platform (3) carrying the detector head and the sample holder mounting is placed on a vibration damping stack (12) [Fig. 5(b)]. The stack consists of six stainless steel plates separated by Viton plates of 5 mm thickness. The Cu platform is connected to the uppermost plate of the stack with four support columns (13). To preserve the damping quality of the Viton material, which becomes stiff at cryogenic temperatures, it is desirable to reduce the thermal contact between the cooled Cu platform and the vibration damping stack. Thus, the support columns connecting these two components were designed in a form of thin-walled stainless steel tubes providing low thermal conductance.

The adjustment of the vertical position of the microcalorimeter to the nonvariable height of the molecular beam is realized by three alignment screws, as in (14).

E. Effusive molecular beam

The molecular beam is designed to provide well-defined, constant, homogeneous, and clean gas flux and to allow fast and variable chopping of the beam flux on a time scale of a few hundredths of a millisecond. In order to ensure a homogeneous spatial profile of the gas flux on the sample surface, the molecular beam was placed as close as possible to the sample surface (4 mm from the outer beam aperture to the sample surface). This geometrical arrangement minimizes the divergence of the gas flux that increases with distance, resulting in a nonhomogeneous distribution of the flux intensity over the sample surface. Additionally, an experimental possibility to couple laser light into the beam path is provided, which is necessary for calibration purposes. The molecular beam is mainly an adaptation of the recently developed effusive sourced described in Refs. 15 and 22. A cross section of the molecular beam is shown in Fig. 6.

The molecular beam is produced by a differentially pumped source based on a glass capillary array (GCA) (Galileo, 50 μm channel diameter, 1 mm thickness) (1), which is located 200 mm from the sample surface. To process the GCA, it was sealed with lacquer, cut from a larger piece, and

Downloaded 25 May 2011 to 141.14.132.216. Redistribution subject to AIP license or copyright; see http://rsi.aip.org/about/rights_and_permissions

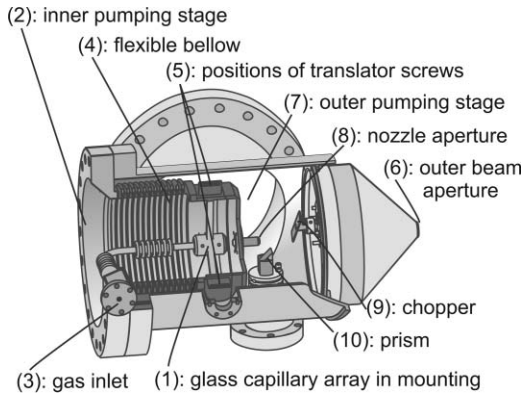

FIG. 6. Molecular beam source: (1) glass capillary array, (2) inner pumping state, (3) gas inlet, (4) flexible bellow, (5) positions of translator screws (the screws are not shown), (6) outer beam aperture, (7) outer pumping stage, (8) nozzle aperture, (9) chopper, and (10) prism.

milled into a disk of 10 mm diameter. After processing, the protective sealing was removed and the device was mounted onto the source tube using Teflon gaskets with an opening of 4 mm diameter. The GCA is mounted in the inner pumping stage (2) differentially pumped by a 500 l/s TMP (Pfeiffer, TMU 521 P) and connected to a gas handling system (3) via a flexible stainless steel hose. The inner pumping stage is mounted on a flexible bellow (4) and can be adjusted by two translator-screws (5) allowing for beam alignment. In order to maximize the pumping speed and to minimize the distance to the exit beam aperture (6), the outer pumping stage (7) was constructed as an integral part of the adsorption/reaction chamber. The second differential stage is pumped by a 500 l/s TMP (Pfeiffer, TMU 521 P). The pressure of both differential stages is measured by cold cathode ion gauges.

After exiting the inner pumping stage through a nozzle aperture (8) of 4 mm diameter, the molecular beam enters the outer pumping stage, where it can be modulated by means of a chopper (9). The beam chopper is a rectangular sheet of Al metal plate, which is driven by a UHV-compatible stepper motor (AML, B14.1). The chopper is fully remote controlled (using LABVIEW software) and allows arbitrary opening times of at least 150 ms. The chopper position, at which the chopper blade blocks the molecular beam, can be controllably set by detecting the opening/closing of a magnetic switch, which consists of small magnets mounted to the ends of the chopper blade.

For the absolute calibration of the pyroelectrically measured adsorption energies, the laser beam is coupled into the molecular beam path using a prism (10). The prism is fixed on a translational feedthrough and can be positioned in the outer pumping stage either below the inner aperture (8) or in front of it. The former position is the working position for the adsorption experiments, allowing the beam of gas molecules to pass through the entire beam path. The latter position is used during the signal intensity calibration, when the laser light is guided into the molecular beam path (for more details of the calibration system, see Sec. II G).

The backing pressure of the GCA is typically set to between 0.001 and 1 mbar, depending on the molecular flux needed for calorimetric measurements. Two gas lines are connected to the tube that delivers gas to the GCA; each of these has an inline electropneumatic valve allowing for complex gas mixtures or fast switching of the gas used to generate the molecular beam. Each gas line has an independent pressure control unit, which controls the backing pressure and consists of an upstream flow control valve (MKS, 248 A, maximum flow rate of 10 sccm nitrogen), a capacitance manometer (MKS, Baratron 122), and a pressure controller (MKS, Type 250).

F. Molecular beam monitor

Accuracy in the determination of the molecular flux and its spatial distribution requires reliable measurement of the beam intensity and its profile. We have, therefore, setup a beam monitor on the principle of an accumulation detector [(5) in Fig. 4] that is an adaption of the beam monitor described previously.[22]

The beam monitor is based on a high accuracy ion gauge (Granville-Phillips, 370 Stabil-Ion) mounted to a stainless steel tube 490 mm long with a diameter of 14 mm. At the front end of the tube, a stainless steel plate is mounted, which has a 1 mm diameter hole in its center. This orifice allows molecules from the beam to enter the detector volume. The assembly is mounted on a manipulator with three translational degrees of freedom. This manipulator is attached to the rotatable platform allowing the beam monitor to be positioned exactly in the sample position for adsorption/reaction experiments. In the working position, the orifice of the beam monitor is placed perpendicular to the incoming molecular beam (and parallel to the sample surface).

The molecular beam entering the aperture causes a pressure rise inside the detector volume. After equilibration of the incoming/outgoing effusive flux from the detector volume, a constant pressure is reached that can be used to calculate the absolute beam flux by the following relation: $dN_{out}/dt = p/\sqrt{2\pi MkT}$, where N_{out} is the number of molecules passing the beam monitor aperture, p is the pressure in the detector volume, M is the mass of the molecule, k_B is the Boltzmann constant, and T is the temperature of the detector.

The high stability pressure gauge has an accuracy of 4% and a repeatability of 1.1%. Typically, the background pressure in the detector is about 5×10^{-9} mbar, so the minimum detectable pressure change is $\sim 1 \times 10^{-11}$ mbar. For Ar this corresponds to a resolution of 2×10^{9} molecules $cm^{-2}\,s^{-1}$ in flux.

G. Energy calibration system

Absolute energy calibration of the calorimeter is realized using light pulses from a He–Ne laser (Linos, 632.8 nm, 2 mW, continuous wave) in a procedure previously described by Stuckless *et al.*[2] It is important for the calibration that the laser and the molecular beam have the same spatial and temporal profiles. Figure 7 shows a schematic representation of the energy calibration system installed in the present experimental setup. The laser light is spread and collimated by means of a lens system (1) and then directed to one of six

Downloaded 25 May 2011 to 141.14.132.216. Redistribution subject to AIP license or copyright; see http://rsi.aip.org/about/rights_and_permissions

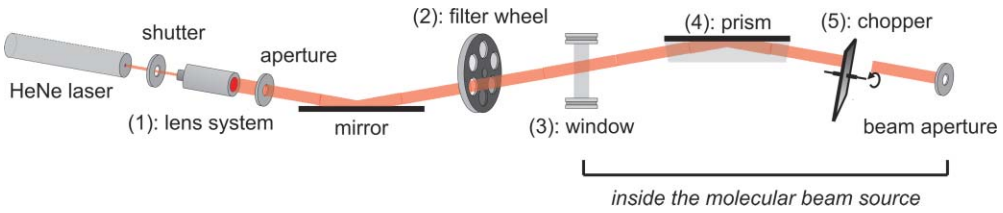

FIG. 7. (Color online) Scheme of the laser calibration system. The labeled components are: (1) lens system, (2) wheel carrying the neutral density filters, (3) chamber window, (4) prism, and (5) chopper.

optical neutral density filters mounted in a rotatable wheel (2). This motorized wheel allows reproducible laser power attenuation with a transmission of 100%, 28.5%, 10.0%, 7.9%, 6.8%, and 5.3%. The attenuated laser beam is passed through a window (3) into the molecular beam source, where it impinges onto a prism (4) installed on a linear translator [the same prism is indicated as (10) in Fig. 6]. During the calibration procedure the prism is temporarily placed directly in the beam path. The laser light is reflected by the prism down the molecular beam path so that the same beam chopper (5) cuts the laser beam into pulses in the same way as the molecular beam. In this manner the detector response in real adsorption measurement can be directly compared to the signal from heating by laser pulses of known energy, provided that the full heat deposition occurs on a time scale that is shorter than the characteristic time of the detection system.[2] The irreproducibility of the linear translator used to position the prism results in variations of the laser power at the sample; therefore, the absolute laser power is measured in each experiment by an *in situ* photodiode [Silicon Sensor, PS95-4; (4) in Fig. 4] that an be positioned in front of the molecular beam by rotating the rotatable platform [(2) in Fig. 4].

III. SYSTEM PERFORMANCE

A. Energy calibration system

Absolute energy calibration requires determining the contact value of the pyroelectric detector, which is defined as the voltage produced by the pyroelectric ribbon per unit of absorbed energy ($V/J_{adsorbed}$). The contact value has to be measured for every sample/ribbon contact because the mechanical/thermal contact is not reproducible (see below). In the calibration procedure, the pulses of laser light impart onto the sample and a fraction of this light absorbs. The power of the laser is adjustable using optical neutral density filters (described in Sec. II G). The fraction of the absorbed laser light depends on the sample's reflectivity at 632.8 nm, which is measured *in situ* (described in Sec. II B). The laser power and the sample's reflectivity are used to calculate the absolute amount of absorbed energy per laser pulse, which is related to the measured voltage produced by the pyroelectric detector. Therefore, precise quantification of the absorbed energy requires accurate measurement of the laser power. In our experimental setup, laser transmission through the beam line is measured *in situ* by direct irradiation of a photodiode (Silicon Sensor, PS95-4). The laser power drifts by $<0.07\%$ in 10 min once the He–Ne laser has warmed-up ($\sim$2 h after powering on). The length of the pulse in time remains constant within the time resolution of the photodiode (rise time of $\sim$1 ms). The *in situ* photodiode is referenced to another absolutely calibrated photodiode (Thorlabs, FDS1010, 350.3 mA/W at 632.8 nm, 95% interval uncertainty: $\pm 0.1\%$) giving an absolute sensitivity of 2.1 ± 0.1 μW/V. Six filters outside the vacuum chamber are used to attenuate the laser power intensity in the range of 1–30 μW (see Sec. II G for the transmission coefficients). The corresponding minimum pulse energy, which can be obtained with the laser power of 1 μW and a beam modulation time of 150 ms, is to 150 nJ (additional filters could be used to further attenuate the beam if necessary).

An example of the calorimeter response for three different laser powers (adsorbed energies of 2831, 793, and 150 nJ) is shown in Fig. 8(a). The peak height of the calorimeter signal, which is proportional to the voltage generated by the pyroelectric ribbon[2], shows a linear dependence on the absorbed energy in agreement with the previous report on this type of detector.[2] The proportionality of the detection response to absorbed energy has also been proven for the entire adsorbed energy range of 150–2831 nJ/pulse. A corresponding plot of the calorimetric signal amplitude as a function of the absorbed energy is shown in Fig. 8(b).

We estimated the calorimeter sensitivity by applying 100 laser pulses of known intensity (245 nJ of absorbed energy per pulse) to the sample surface and evaluating the pulse-to-pulse standard deviation of the voltage signal produced by the pyroelectric ribbon, which was found to be 15 nJ. In the other series of experiments, the laser intensity was varied in the range of 190–3600 nJ/pulse and 20 pulses were used for each energy to determine the pulse-to-pulse standard deviation, which was found to lie between 4 and 16 nJ. These values (all at room temperature) are close to the pulse-to-pulse standard deviations (19 nJ at 298 K and 35 nJ at 100 K) previously reported by Lew *et al.*[4] for the same type of detector and the similar energy range (2200 nJ/ laser pulse). For CO adsorption on Pt(111), the energy input of 15 nJ (or 120 nJ cm^{-2}) corresponds to adsorption of less than 1.5×10^{12} CO molecules cm^{-2} or less than 0.1% of a monolayer (one monolayer $= 1.5 \times 10^{15}$ cm^{-2}).

B. Effusive molecular beam

A variable molecular beam flux is achieved by varying the backing pressure of the beam source. Figure 9 shows the centerline intensity for an Ar beam as measured using the beam monitor that was placed in front of the outer

Downloaded 25 May 2011 to 141.14.132.216. Redistribution subject to AIP license or copyright; see http://rsi.aip.org/about/rights_and_permissions

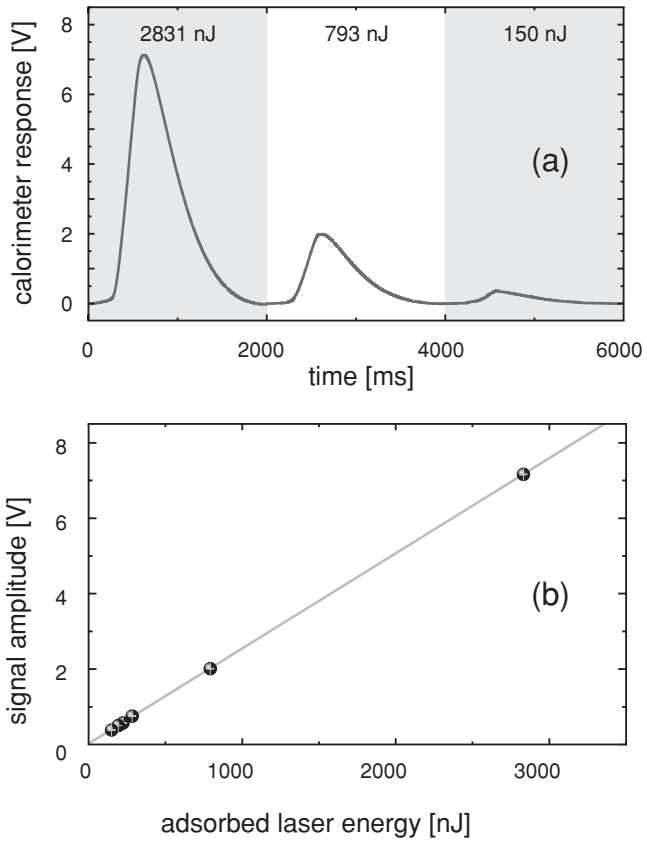

FIG. 8. (a) The calorimetric response to a train of laser pulses of different intensities onto a 1 μm thick Pt(111) sample at 300 K. (b) Peak-to-peak output voltage vs absorbed heat input to the sample showing the linearity of the detector response.

molecular beam aperture. It should be noted that the effusive beam expansion starts from low pressure conditions with nearly noninteracting gas phase particles so that this type of expansion is gas independent. In the backing pressure range from 1×10^{-3} to 2×10^{-1} mbar, the molecular flux increases linearly with the increasing pressure. Above 2×10^{-1} mbar, the flux intensity levels off at the value of $\sim 1.5 \times 10^{15}$ molecules $\mathrm{cm}^{-2}\,\mathrm{s}^{-1}$, which is the maximum beam intensity in the present experimental setup. This intensity corresponds to deposition of about 2 ML of CO molecules on Pt(111) per second. The existence of the highest limit for the beam intensity can be most likely explained by reaching a nontransparent mode of operation of the GCA when the backing pressure is increased.[23] In principle there is no lower limit to the beam intensity. However, the components of the source pressure regulation limit the range of controllable values to above 5×10^{12} molecules $\mathrm{cm}^{-2}\,\mathrm{s}^{-1}$.

Variable time modulation of the molecular flux by means of a mechanical chopper allows the production of beam pulses of arbitrary length with the minimum pulse length of 150 ms. The pulse length is measured by pulsing the laser onto the photodiode. No variations of the pulse length within the time resolution of 1 ms were revealed. When the molecular beam is blocked by the chopper, a leakage of about 1% of the unblocked beam intensity is observed using the QMS, which is caused by the increased background pressure in the outer pumping stage.

Figure 9(b) presents a 3D beam profile at a source pressure of 3.75×10^{-2} mbar. For this measurement, the beam monitor was placed in front of the outer molecular beam aperture, which has a diameter of 4 mm, and moved in the plane parallel to the sample position. It should be noted that the presented beam profile is convoluted with the beam aperture of 1 mm in diameter. The measured beam profile has a diameter of (4 ± 0.1) mm, which coincides with the desired value. At the fixed position of the beam monitor, fluctuations of the beam intensity are typically below the detection limit of the ionization gauge. When the position of the beam monitor is changed during the measurement to scan the beam profile, the variation of the beam intensity over the central plateau between different beam monitor positions coincides with the stated measurement repeatability of the gauge manufacturer of 3%. Both observations demonstrate the homogeneous and stable flux of gaseous species delivered to the sample surface.

C. Reflectivity measurement in the preparation chamber

He–Ne laser light at 632.8 nm is used to calibrate microcalorimeter's response to the energy released by adsorbing molecules. Therefore, it is critical to know (to high-accuracy,

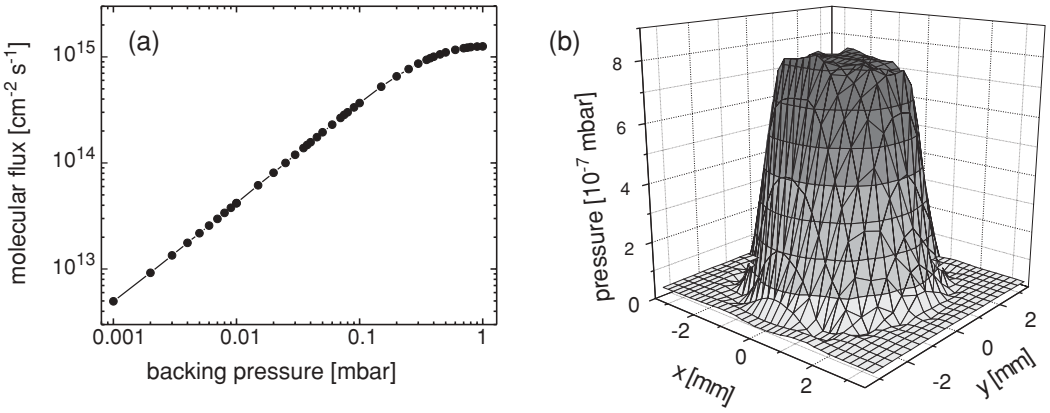

FIG. 9. (a) Intensity of the effusive beam source plotted as a function of the backing pressure. (b) Beam profile at the sample position obtained at the backing pressure 3.75×10^{-2} mbar.

Downloaded 25 May 2011 to 141.14.132.216. Redistribution subject to AIP license or copyright; see http://rsi.aip.org/about/rights_and_permissions

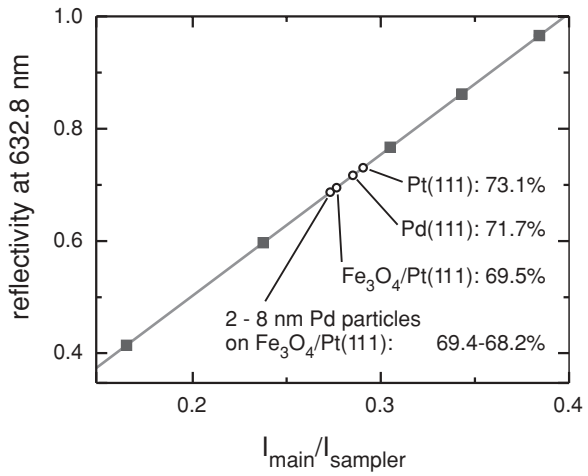

FIG. 10. The calibration curve showing the dependence of the reflectivity of the calibration mirrors on the photodiode intensity ratio $I_{main}/I_{sampler}$ measured with He–Ne laser at 632.8 nm (black squares, see the explanation in the text). The positions of the reflectivities for different samples are indicated with the open circles.

less than a few percent absolute error) the reflectivity of the sample at 632.8 nm, which we measure in a separate laser system in the preparation chamber (see Sec. II B for details). The laser beam is split by a beam splitter into two parts and ~30% of the laser beam is directed to a photodiode [sampler photodiode (5) in Fig. 3]. The ratio of the intensities $I_{main}/I_{sampler}$, measured by the main and the sampler photodiodes, respectively, is directly proportional to the reflectivity of the sample. To determine the proportionality factor, we measure the ratio $I_{main}/I_{sampler}$ for calibration mirrors of known reflectance: 41.4 ± 0.4%, 59.7 ± 0.9%, 76.7 ± 1.1%, 86.2 ± 0.2%, and 96.6 ± 0.1%. Figure 10 shows the reflectivity of the five calibration mirrors at 632.8 nm plotted as a function of the ratio $I_{main}/I_{sampler}$ (black squares). The observed linear dependence of reflectivity on the intensity ratio validates the use of this calibration procedure. The slope of this calibration curve was used to calculate the reflectivity of the sample surfaces used in our studies. Additional data points in Fig. 10 (stars) show the reflectivity of pristine single crystal surfaces Pt(111) and Pd(111) as well as the thin Fe_3O_4 (~10 nm thickness) oxide layer prepared on top of Pt(111) and the reflectivity of Fe_3O_4 supported Pd nanoparticles (average nanoparticle size range 2–8 nm).[24] These data reveal that preparation of the thin oxide layer, which is only ~10 nm thick, significantly changes the reflectivity of the sample surface. This observation clearly demonstrates the importance of measuring *in situ* the reflectivity of complex model systems, whose structure can only be preserved under UHV conditions.

D. Accuracy and precision of the microcalorimetric measurement

To estimate the error of the calorimetric measurement one needs to consider accuracy and precision of two main independent parts constituting the experiment: the energy measurement and the measurement of the absolute number of adsorbates produced by one gas pulse. Table I summarizes the error values contributing to the overall accuracy and precision

TABLE I. Measurements contributing to the overall accuracy and precision of the microcalorimetric experiment.

Energy measurement	Accuracy and precision	
Photodiode sensitivity	Accuracy: 0.1%	Determined by the National Institute for Metrology (PTB)
	Precision: <0.1%	Standard deviation for 62 000 measurements
Stability of laser power (over 10 min)	Precision: <0.08%	Standard deviation for 60 000 measurements
Reflectivity	Accuracy: <1.3%	Determined using a standard mirror with known reflectivity
On single crystal surfaces	Precision: <0.07%	Error of mean for 20 measurements on Pt(111)
On Fe_3O_4/Pt(111) (thickness ~100 Å)	Precision: ≤1.3%	Maximal variation for three different preparations
Pulse length	Accuracy: ≤0.4%	No variations of the pulse length of 266 ms can be detected with the detection limit of 1 ms
Number of adsorbates		
Molecular beam intensity	Accuracy: 4%	Absolute accuracy of the ion gauge stated by manufacturer
	Precision: <1.1%	Standard deviation from 28 measurements; relates to finding the same working position of the beam monitor
Stability of the molecular beam	Precision: <0.2%	Variation of the molecular beam intensity over time in the same working position of the beam monitor; below the detection limit
Beam profile area	Accuracy: <5%	Estimated from the spatial resolution of the beam monitor (0.1 mm)
Sticking probability	Accuracy: ~2%–6%	see Ref. 17 for details, depends on the gas and the magnitude of the sticking probability
When ≥0.7	Precision: 1.0%	Standard deviation for six independent measurements on CO adsorption on Pt(111)
When ≤0.3	Precision: 30%	Standard deviation for six independent measurements on CO adsorption on Pt(111)

Downloaded 25 May 2011 to 141.14.132.216. Redistribution subject to AIP license or copyright; see http://rsi.aip.org/about/rights_and_permissions

of both parts of the experiment, referring always to the error on a single gas pulse.

Two types of errors are listed in this table: the systematic errors, which are related to accuracy of the measurement, and the statistical errors related to precision. The latter value reflects the reproducibility of the measurement and can be significantly improved by statistical averaging of several measurements. Generally, by performing large number of experiments it is potentially possible to improve the precision to such an extent that it becomes better than the accuracy and does not significantly contribute to the overall error. However, in practice it is not always possible since such improvement requires repeating the measurements on the fully identical surfaces, which are difficult to prepare, especially in the case of the supported model catalysts.

The main source of the errors in the energy measurement is determining the laser energy absorbed by the sample per pulse, which depends on the accuracies of the photodiode sensitivity, the pulse length, and the reflectivity of the sample. The accuracy of the latter parameter (~1.3%) was estimated to have the largest contribution to the total accuracy of the energy measurement. Precision (statistical error) of the reflectivity measurement was found to be considerably better than the accuracy value for the single crystal surfaces. However, the statistical error on a single measurement of the reflectivity of an oxide-supported model catalyst is comparable with the systematic error, meaning that the statistical error considerably contributes to the overall error of the energy measurement for these model catalysts. This observation arises from the fact the reflectivity of the oxide film depends linearly on its thickness.[25] Since the metal deposition rate determining the thickness of the resulting oxide layer can vary slightly from preparation to preparation, the reflectivity may be subject to large statistical errors. (This error is much smaller when measuring on perfectly reproducible surfaces like clean single crystal metals.)

The error of determining the absolute number of adsorbates is defined by the errors of the measurements of the molecular beam flux, the beam profile area, and the sticking coefficient. The accuracy and precision of the latter parameter are gas- and coverage-dependent values. As discussed by King and Wells in detail,[17] the accuracy of the sticking coefficient is set by the linearity of the pressure gauge (in our case—QMS) and the position of the zero-sticking reference. For the gases not sticking on the chamber walls, the accuracy was estimated to amount to a few percent. However, the accuracy can decrease if the gas sticks on the walls or other components of the UHV chamber. To test our experimental setup, we determined the statistical error of the sticking coefficient measurement for CO adsorption on Pt(111) for six independent measurements. We found that the relative standard deviation depends on the magnitude of the sticking coefficient: it amounts to ~1% if the absolute value of the sticking coefficient is high (>0.7) and to ~30% for the low sticking coefficient values (<0.3). The large statistical error for the low sticking coefficients arises mainly from the error of determining the position of the zero-sticking reference. It should be noted that the statistical error of ~30% has the largest contribution into the overall error for the case of the low sticking coefficients. Here, large data sets need to be obtained in order to accurately determine the amount of adsorbed molecules.

The overall accuracy of the adsorption energy measurement (kJ per mole adsorbed) is estimated to be in the range of 7%–9% for a single measurement adsorption energy versus coverage on such a model oxide-supported catalyst for high sticking coefficient gases that do not stick on the chamber walls.

IV. TEST MEASUREMENTS: HEATS OF COADSORPTION ON Pt(111) AT 300 AND 130 K

In our new experimental setup, a high-flux stable molecular beam can be generated using both light (high vapor pressure, such as CO) and heavy (low vapor pressure, such as benzene) gases and the measurements can be carried out in a broad temperature range (100–300 K). This allows us to considerably extend the range of the adsorption systems and experimental conditions as compared to the already available microcalorimetric data, which are restricted either to the adsorption of high vapor pressure gases in the temperature range 100–300 K (Ref. 4) or to adsorption of both high and low vapor pressure gases at 300 K.[6]

To test the calorimeter we measured CO adsorption on Pt(111) as a detailed function of coverage and compared these results to published microcalorimetric measurements from King's group.[6] Additionally, we investigated CO adsorption at 130 K, which cannot be measured using optical pyrometry. The results are described in detail elsewhere,[25] but we summarize them here to show how the system performs.

Figure 11 shows the response of the pyroelectric ribbon (in mechanical/thermal contact with the single crystal) to pulses of CO molecules adsorbing onto Pt(111) [Fig. 11(a)] and laser pulses [Fig. 11(b)] impinging onto Pt(111). In both cases the length of the pulse was 266 ms. The signals in Fig. 11 are normalized to allow for more convenient comparison of the line shapes. Identical line shapes for the pyroelectric ribbon's response to heat deposited from the laser pulse

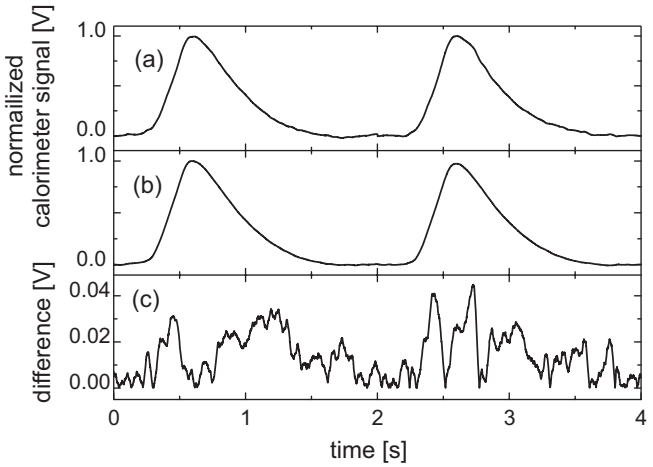

FIG. 11. Comparison of the detector response curves for the energy input upon adsorption of CO molecules (a) and absorption of the laser light (b) on 1 μm thick Pt(111) sample at 300 K, (c) difference between the normalized detector responses shown in (a) and (b), proving negligible line shape difference.

Downloaded 25 May 2011 to 141.14.132.216. Redistribution subject to AIP license or copyright; see http://rsi.aip.org/about/rights_and_permissions

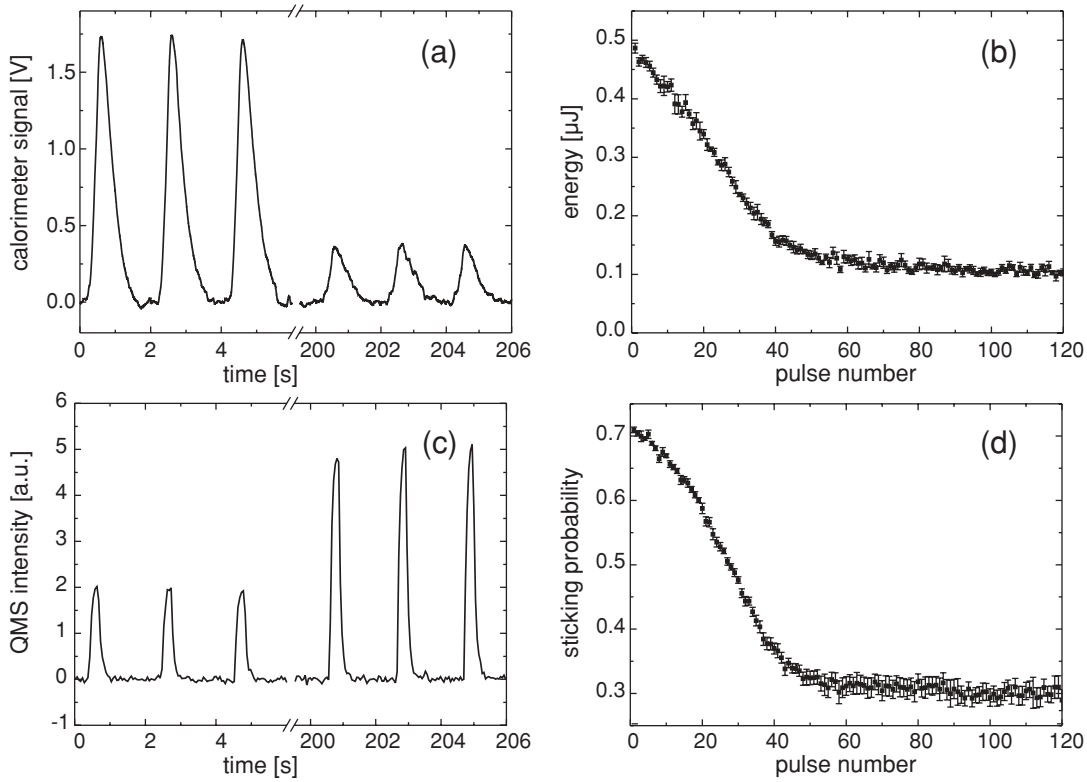

FIG. 12. A typical dataset obtained upon adsorption of CO on 1 μm Pt(111) at 300 K (CO flux: 2.6×10^{13} CO molecules cm^{-2} per pulse or 0.017 ML/pulse). (a) The detector response from a train of CO pulses, (b) the energy released per CO pulse plotted as a function of pulse number, (c) time evolution of the QMS signal at amu 28 used for calculated the sticking probability, and (d) the sticking probability plotted as a function of pulse number.

and molecular adsorption is required to achieve the highest-accuracy in energy calibrations.[1,18] The difference between the two normalized signals shown in Fig. 11(c) demonstrates that this condition is reasonably fulfilled (<4% deviation) for CO adsorption on Pt(111) at 300 K.

A typical complete calorimetric data set is shown in Fig. 12. Figure 12(a) shows the response of the pyroelectric ribbon plotted as a function of time due to the adsorption of CO onto Pt(111) at 300 K. The energy released per CO pulse is presented as a function of the pulse number in Fig. 12(b). The data in Fig. 12(a) were obtained in a single measurement; the energies presented in Fig. 12(b) are an average from six measurements with the error bars being statistical errors of the mean. The molecular beam flux was 9.7×10^{13} CO molecules cm^{-2} s^{-1}, which in combination with the pulse length of 266 ms results in the amount of 2.6×10^{13} CO molecules cm^{-2} supplied to the surface per molecular beam pulse. At the beginning of the exposure the initial adsorption energy on the clean Pt(111) surface is high (468 ± 8 nJ/pulse), which decreases with increasing CO exposure and levels off at a constant nonzero value after about 50 CO pulses. Figure 12(c) shows the time evolution of the QMS signal at 28 amu, corresponding to CO, recorded simultaneously with the calorimetric measurement. This trace is used to calculate

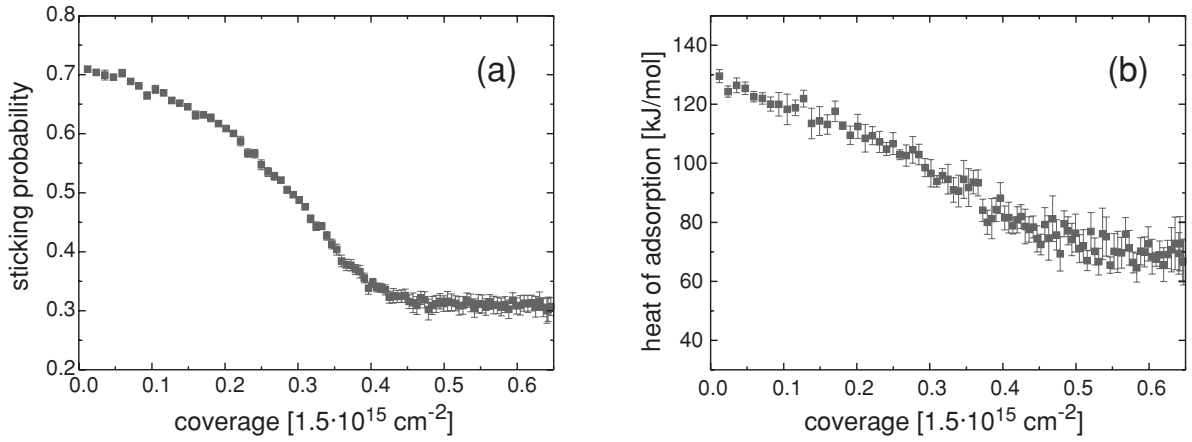

FIG. 13. Sticking probability and adsorption heat of CO on Pt(111) at 300 K plotted as a function of CO surface coverage.

Downloaded 25 May 2011 to 141.14.132.216. Redistribution subject to AIP license or copyright; see http://rsi.aip.org/about/rights_and_permissions

the sticking probability of CO on Pt(111) via the King–Wells method,[17] which is displayed in Fig. 12(d) as a function of CO pulse number. The initial sticking probability on the clean sample is 0.710 ± 0.005 at 300 K in agreement with the values ranging from 0.6 to 0.8 reported in the literature,[26–29] and decreases to a constant value of 0.31 ± 0.01 after ~60 CO pulses. It should be noted that in a microcalorimetry experiment carried out under the conditions at which the gas can desorb there are constant nonzero sticking probability and adsorption heat, even after the apparent saturation of the surface at high exposures is reached. This effect is a consequence of the fact that the CO saturation coverage depends on the CO pressure in the gas phase:[27,30] it is higher while the surface is exposed to the molecular beam and decreases after the interruption of the beam to the value inherent to UHV conditions. As a consequence, a part of molecules desorbs from the surface between gas pulses and a steady state is reached, in which the adsorption during a gas pulse balances the desorption between gas pulses and leads to an apparent uptake of CO onto the surface in the quasisaturation regime. Similar adsorption–desorption equilibrium in the quasisaturated regime was previously observed in microcalorimetric measurements of CO adsorption onto Pd, Pt, and Ni single crystals[6] and cyclohexene on Pt(111).[18] It has to be noted, however, that the absolute value of the CO sticking coefficient in the quasisaturation regime is subject to large systematic error since the absolute number of adsorbing molecules is small and difficult to measure (see Sec. III). The sticking coefficient measured in such a way allows us to calculate the absolute number of CO molecules that were adsorbed on the surface per single pulse and the CO coverage reached on the surface. By dividing the measured energy input by the absolute number of adsorbed molecules we obtain a heat of CO adsorption in kilojoules per mole inverse, which is plotted as a function of surface coverage in Fig. 13. The measured initial adsorption heat amounts to ~130 ± 2 kJ mol^{-1}, which continuously decreases to the value of 70 ± 5 kJ mol^{-1} reached in the quasisteady state regime. The adsorption heat remains constant starting from the coverage of about 0.5 ML (referred to the 1.5×10^{15} Pt surface atoms cm^{-2}), which is in a excellent agreement for the CO saturation coverage of 0.5 ML on Pt(111) reported previously.[27,31,33] Two reasons account for the decreasing adsorption enthalpy with growing CO coverage: intermolecular repulsion of neighboring CO molecules and increasing competition for the *d*-electrons of Pt participating in the CO–Pt bonding.[32]

In the literature, there is no general agreement on the value of the adsorption energy of CO in the initially clean Pt(111). In the early work of Ertl *et al.*[33] the initial CO adsorption energy was found to be 135 ± 4 kJ mol^{-1}, as derived from isosteric heat of adsorption measurements. Further experimental studies, including TPD,[29,33–35] equilibrium adsorption isotherms in combination with He^+ ion scattering,[36] and modulated molecular beam studies,[29] report the CO adsorption energy (in the low-coverage limit) to be in the range of 126–138 kJ mol^{-1}. In the direct calorimetric measurement by King *et al.* a significantly higher value of 187 ± 11 kJ mol^{-1} was observed.[6] It is clear that the value 130 ± 2 kJ mol^{-1} obtained in this study is in much better agreement with the values previously measured by indirect methods than with the value measured by SCAC in the King's group. One of the possible explanations of this discrepancy can be the different value of reflectivity of Pt(111) that was used to calculate the adsorption energy: while 66% reflectivity[37] was assumed in King's study (based on the literature reflectivity value, see references in Ref. 37), we used 73% reflectivity value determined in our *in situ* setup for reflectivity measurement. If the value 187 kJ mol^{-1} is recalculated with the reflectivity of Pt(111) 73%, one obtains the energy 149 kJ mol^{-1}, which is closer to the value measured in this study and by other indirect methods.

Figure 14 shows the results of the calorimetric measurement for CO adsorption on Pt(111) at 130 K. The sticking probability is plotted as a function of CO surface coverage in Fig. 14(a); the adsorption energy of CO is displayed in Fig. 14(b) as a function of CO coverage. Both plots are an average of nine independent measurements. The dependence of the sticking probability on coverage is in good qualitative agreement with CO adsorption data obtained at 300 K. Quantitatively, the initial sticking coefficient nearly coincides (within 1.5% at 0.01 ML) with that one measured at 300 K, but as the coverage increases it remains consistently higher than the room temperature value until the quasisaturation

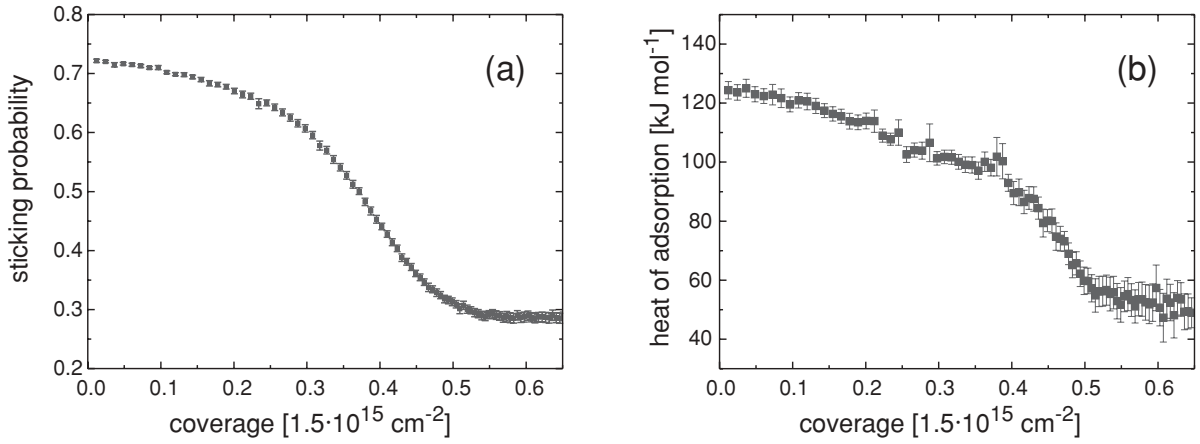

FIG. 14. CO sticking probability (a) and adsorption heat (b) on Pt(111) at 130 K plotted as a function of CO surface coverage.

Downloaded 25 May 2011 to 141.14.132.216. Redistribution subject to AIP license or copyright; see http://rsi.aip.org/about/rights_and_permissions

regime is reached. The initial adsorption energies and their dependence on the CO coverage were found to be very similar for both temperature regimes (130 ± 3 kJ mol^{-1} at 300 K vs 124 ± 3 at 130 K). In the forthcoming paper we will discuss the origin of the observed phenomena in more detail.[25] Here, we mainly want to demonstrate that the statistical scatter of the data obtained under low-temperature conditions is as good as at room temperature (3 kJ mol^{-1} both at 300 and 130 K). We attribute this fact to the exceptionally good thermal stability of the whole microcalorimeter assembly achieved in the presented setup (<0.4 mK over tens of minutes[38]).

Finally, the detection limit of the calorimeter for CO molecules on clean Pt(111) was estimated to be about 1.5×10^{12} molecules cm^{-2} s^{-1}, which corresponds to an energy input of about 15 nJ or 120 nJ/cm^2, taking the area of 0.126 cm^2 exposed to the adsorbates into account.

ACKNOWLEDGMENTS

The authors would like to thank J. Libuda and D. Starr for valuable discussions. J.A.F. would like to acknowledge the Center for Nanotechnology at the UW for a National Science Foundation (NSF)-supported IGERT Award (DGE-0504573). C.T.C. acknowledges the U.S. Department of Energy (DOE) Office of Basic Energy Sciences, Chemical Sciences Division for partial support of this work. S.S. acknowledges Robert Bosch Foundation.

[1] C. E. Borroni-Bird and D. A. King, Rev. Sci. Instrum. **62**, 2177 (1991).
[2] J. Stuckless, N. Frei, and C. T. Campbell, Rev. Sci. Instrum. **69**, 2427 (1998).
[3] C. T. Campbell and O. Lytken, Surf. Sci. **603**, 1365 (2009).
[4] W. Lew, O. Lytken, J. A. Farmer, M. C. Crowe, and C. T. Campbell, Rev. Sci. Instrum. **81**, 24102 (2010).
[5] H. M. Ajo, H. Ihm, D. E. Moilanen, and C. T. Campbell, Rev. Sci. Instrum. **75**, 4471 (2004).
[6] W. Brown, R. Kose, and D. A. King, Chem. Rev. **98**, 797 (1998).
[7] N. Krishnankutty and M. A. Vannice, J. Catal. **155**, 312 (1995).
[8] M. Bäumer and H.-J. Freund, Prog. Surf. Sci. **61**, 127 (1999).
[9] C. R. Henry, Surf. Sci. Rep. **31**, 231 (1998).
[10] D. R. Rainer and D. W. Goodman, J. Mol. Catal. A: Chem. **131**, 259 (1998).
[11] H.-J. Freund, Surf. Sci. **500**, 271 (2002).
[12] H.-J. Freund, Angew. Chem., Int. Ed. **36**, 452 (1997).
[13] T. Schalow, B. Brandt, D. E. Starr, M. Laurin, S. K. Shaikhutdinov, S. Schauermann, J. Libuda, and H.-J. Freund, Angew. Chem., Int. Ed. **45**, 3693 (2006).
[14] H.-J. Freund and G. Pacchioni, Chem. Soc. Rev. **37**, 2224 (2008).
[15] H. Ihm, H. M. Ajo, J. M. Gottfried, P. Bera, and C. T. Campbell, J. Phys. Chem. B **108**, 14627 (2004).
[16] S. Cverny, Surf. Sci. Rep. **26**, 1 (1996).
[17] D. A. King and M. Wells, Surf. Sci. **29**, 454 (1972).
[18] O. Lytken, W. Lew, J. Harris, E. Vestergaard, J. M. Gottfried, and C. T. Campbell, J. Am. Chem. Soc. **130**, 10247 (2008).
[19] Produced by Jacques Chevalier, Aarhus University.
[20] J. T. Stuckless, N. A. Frei, and C. T. Campbell, Sens. Actuators B **62**, 13 (2000).
[21] *Handbook of Chemistry and Physics*, edited by D. R. Lide (CRC Press, Boca Raton, FL, 2009), p. 135.
[22] J. Libuda, I. Meusel, J. Hartmann, and H.-J. Freund, Rev. Sci. Instrum. **71**, 4395 (2000).
[23] *Atomic and Molecular Beam Methods*, edited by G. Scoles (Oxford University Press, New York and Oxford, 1988), Vol. 1, p. 254.
[24] The reflectivity measurements were performed on the flat thick (1 mm) samples. The thin (1 μm) samples cannot be used for the *in situ* reflectivity measurements, since their surface is not macroscopically flat.
[25] J.-H. Fischer-Wolfarth, J. M. Flores-Camacho, J. A. Farmer, C. T. Campbell, S. Schauermann, and H.-J. Freund (unpublished).
[26] H. Steininger, S. Lehwald, and H. Ibach, Surf. Sci. **123**, 264 (1982).
[27] J. Liu, M. Xu, T. Nordmeyer, and F. Zaera, J. Phys. Chem. **99**, 6167 (1995).
[28] Y. Yeo, L. Vattuone, and D. A. King, J. Chem. Phys. **106**, 392 (1997).
[29] C. T. Campbell, G. Ertl, and H. Kuipers, J. Segner, Surf. Sci. **107**, 207 (1981).
[30] S. R. Longwitz, J. Schnadt, E. K. Vestergaard, R. T. Vang, E. Lægsgaard, I. Stensgaard, H. Brune, and F. Besenbacher, J. Phys. Chem. B **108**, 14497 (2004).
[31] J. Davies and P. Norton, Nucl. Instrum. Methods **168**, 611 (1980).
[32] J.-H. Fischer-Wolfarth, J. A. Farmer, J. M. Flores-Camacho, A. Genest, I. V. Yudanov, N. Rösch, C. T. Campbell, S. Schauermann, and H.-J. Freund, Phys. Rev. B **81**, 241416(R) (2010).
[33] G. Ertl, M. Neumann, and K. M. Streit, Surf. Sci. **64**, 393 (1977).
[34] D. Collins and W. Spicer, Surf. Sci. **69**, 85 (1977).
[35] R. McCabe and L. Schmidt, Surf. Sci. **65**, 189 (1977).
[36] B. Poelsema, R. L. Palmer, and G. Comsa, Surf. Sci. **136**, 1 (1984).
[37] Obtained from J. H. Weaver, Department of Chemical Engineering and Materials Science, University of Minnesota.
[38] The upper limit for the temperature stability was estimated from the PPSD 4–16 nJ, mass and the specific heat capacity of the sample.

Downloaded 25 May 2011 to 141.14.132.216. Redistribution subject to AIP license or copyright; see http://rsi.aip.org/about/rights_and_permissions